

Three-dimensional simulations of multiple protoplanets embedded in a protostellar disc

P. Cresswell and R. P. Nelson

Astronomy Unit, Queen Mary, University of London, Mile End Rd, London, E1 4NS, U.K.

Received December 2007 / Accepted February 2008

ABSTRACT

Context. Theory predicts that low-mass protoplanets in a protostellar disc migrate into the central star on a time scale that is short compared with the disc lifetime or the giant planet formation time scale. Protoplanet eccentricities of $e \gtrsim H/r$ can slow or reverse migration, but previous 2D studies of multiple protoplanets embedded in a protoplanetary disc have shown that gravitational scattering cannot maintain significant planet eccentricities against disc-induced damping. The eventual fate of these systems was migration into the central star.

Aims. Here we simulate the evolution of low-mass protoplanetary swarms in three dimensions. The aim is to examine both protoplanet survival rates and the dynamical structure of the resulting planetary systems, and to compare them with 2D simulations.

Methods. We present results from a 3D hydrodynamic simulation of eight protoplanets embedded in a protoplanetary disc. We also present a suite of simulations performed using an N -body code, modified to include prescriptions for planetary migration and for eccentricity and inclination damping. These prescriptions were obtained by fitting analytic formulae to hydrodynamic simulations of planets embedded in discs with initially eccentric and/or inclined orbits.

Results. As was found in two dimensions, differential migration produces groups of protoplanets in stable, multiple mean-motion resonances that migrate in lockstep, preventing prolonged periods of gravitational scattering. In almost all simulations, this leads to large-scale migration of the protoplanet swarm into the central star in the absence of a viable stopping mechanism. The evolution involves mutual collisions, occasional instances of large-scale scattering, and the frequent formation of the long-lived, co-orbital planet systems that arise in $> 30\%$ of all runs.

Conclusions. Disc-induced damping overwhelms eccentricity and inclination growth due to planet-planet interactions, leading to large-scale migration of protoplanet swarms. Co-orbital planets are a natural outcome of dynamical relaxation in a strongly dissipative environment, and if observed in nature would imply that such a period of evolution commonly arises during planetary formation.

Key words. planet formation- extrasolar planets- -orbital migration-protoplanetary disks

1. Introduction

The observed lower limits on extrasolar planet mass are continuing to decrease, while at the same time the number of known multiple planet systems is continuing to grow (Rivera et al. 2005; Lovis et al. 2006; Udry et al. 2007). Multiple planet systems containing sub-Neptune mass planets are now being discovered. Missions such as CoRoT and Kepler are expected to discover further sub-Neptune mass planets beyond the reach of current observations, leading the way toward finding planetary systems more like our own.

Formation of a planetary system is believed to involve accretion within a protoplanetary disc, involving essentially three steps: coagulation of dust grains into small (~ 1 km) planetesimals; runaway growth of planetesimals into larger (~ 100 – 1000 km) protoplanets; oligarchic growth by planetesimal accretion into larger planetary cores. Those cores forming beyond the snow line are expected to reach masses of $\sim 10 M_{\oplus}$, accreting a gaseous envelope to become gas giants if they form before disc dispersal, or ice giants should they form late in the disc's lifetime (Bodenheimer & Pollack 1986; Pollack et al. 1996). Smaller, Mars-mass bodies result from oligarchic growth in the terrestrial zone, and accrete *via* giant impacts to form an inner system of rocky, terrestrial-mass planets (Chambers & Wetherill 1998).

One of several problems associated with this picture is the rapid inward migration experienced by a protoplanet due to the gravitational interaction between it and the gaseous disc (Ward 1997; Tanaka et al. 2002). In particular, understanding the formation of giant planets, which must spend more than 10^6 years in the disc in order to accrete a gas envelope, remains an unsolved problem. Their solid cores have migration times shorter than both the gas accretion time scale and the disc life time (Papaloizou & Nelson 2005). Referred to as type I migration, this drift makes it hard to understand how gas giants can form at all without being accreted by the central star. Solving the type I problem remains an active area of research, and recently suggested remedies include: stochastic migration in a turbulent disc (Nelson & Papaloizou 2004; Nelson 2005); corotation torques operating in a region of positive gradient in disc surface density (Masset et al. 2006); corotation torques in radiatively inefficient discs (Paardekooper & Mellema 2006). In this paper we further explore the role of protoplanet scattering (Cresswell & Nelson (2006) — hereafter Paper I).

Many authors have examined the interactions of multiple planetary embryos, or fully formed planets, within protoplanetary discs. Numerical simulations of the oligarchic growth phase have been used to examine the interactions of planetary embryos (Kokubo & Ida 2000; Thommes et al. 2003). McNeil et al. (2005) found that a proto-terrestrial system may form against type I migration by enhancing the disc mass by a factor of 2–4.

Resonant capture between two planets in the 1–20 M_\oplus range has been studied by Papaloizou & Szuszkiewicz (2005). Thommes (2005) suggests that the formation of the first giant planet may be a significant step in the formation of a planetary system, by capturing smaller cores in resonance and preventing further type I migration. Previously, pairs of giant planets in resonance have been examined, often with direct application to a specific system such as GJ 876 (Snellgrove et al. 2001; Kley et al. 2005).

One area that has not been addressed to the same depth is the issue of how a swarm of protoplanetary cores, of Earth mass and above, will evolve under the influence of a surrounding protoplanetary disc. Models of oligarchic growth (Kokubo & Ida 2000; Thommes et al. 2003) predict that a number of cores should form coevally, separated in radius by ~ 8 mutual Hill radii. Differential type I migration may cause these bodies to undergo close encounters, leading to gravitational scattering and the pumping of eccentricities.

Papaloizou & Larwood (2000) found that type I migration can be slowed or reversed when a protoplanet embedded in a disc achieves an eccentricity $e \gtrsim 1.1H/r$, where H/r is the disc's scale height-to-radius ratio, raising the possibility of the mutual interactions of a swarm of cores sustaining significant eccentricities and slowing type I migration for at least some of them. In an earlier study, however, using 2D N -body and hydrodynamic models we found that the damping action of the disc is too strong to sustain eccentricities in this manner (see Paper I). Instead the cores form resonant groups and migrate inwards in lockstep. Due to the 2D modelling it is possible that the collision probability was overestimated, removing a higher number of protoplanets than should be properly expected, and the influence of planetary inclinations on reducing the migration rate was neglected.

To address these issues, we perform 3D numerical simulations of swarms of planetary cores embedded in a protoplanetary disc. In the first instance we present the results of a full, 3D hydrodynamic simulation of a protoplanetary disc containing eight protoplanets. This simulation provides a good illustration of the early stages of evolution, but cannot be run for long times. To examine the long term evolution, we also present 3D simulations performed with an N -body code, modified to include prescriptions for migration, and eccentricity and inclination damping. These prescriptions were obtained by fitting analytic formulae to numerous 3D hydrodynamic simulations of protoplanets on eccentric and/or inclined orbits embedded in a protoplanetary disc. The results of these 3D multiplet simulations suggest that gravitational interactions among a swarm remains ineffective at maintaining the requisite eccentricities to slow/stop migration, due to the strong damping from the disc. We also find that many co-orbital planets form naturally from such a migrating population, raising the possibility of their detection among the observed extrasolar hot Neptunes and super-earths.

The plan of this paper is as follows. In Sect. 2 we describe the basic equations of motion. In Sect. 3 we describe the two numerical schemes and provide equations describing the disc's action on the protoplanets. In Sect. 4 we describe the initial conditions. In Sect. 5 we present a hydrodynamic multiple-planet model. In Sect. 6 we present the results obtained from the modified N -body scheme, and discuss the trends and implications of these results. We give our conclusions in Sect. 7.

2. Equations of Motion

An unperturbed protoplanetary disc with constant aspect ratio H/r can be conveniently described using spherical polar coor-

dinates (r, θ, ϕ) with the origin located at the central star. The continuity equation is expressed as

$$\frac{\partial \rho}{\partial t} + \nabla \cdot (\rho \mathbf{v}) = 0, \quad (1)$$

and the three components of the momentum equation are written

$$\frac{\partial (\rho v_r)}{\partial t} + \nabla \cdot (\rho v_r \mathbf{v}) = \frac{\rho(v_\theta^2 + v_\phi^2)}{r} - \frac{\partial p}{\partial r} - \rho \frac{\partial \Phi}{\partial r} + f_r \quad (2)$$

$$\begin{aligned} \frac{\partial (\rho v_\theta)}{\partial t} + \nabla \cdot (\rho v_\theta \mathbf{v}) = & -\frac{\rho v_r v_\theta}{r} + \frac{\rho v_\phi^2 \cot \theta}{r} \\ & -\frac{1}{r} \frac{\partial p}{\partial \theta} - \frac{\rho}{r} \frac{\partial \Phi}{\partial \theta} + f_\theta \end{aligned} \quad (3)$$

$$\begin{aligned} \frac{\partial (\rho v_\phi)}{\partial t} + \nabla \cdot (\rho v_\phi \mathbf{v}) = & -\frac{\rho v_r v_\phi}{r} - \frac{\rho v_\theta v_\phi \cot \theta}{r} \\ & -\frac{1}{r \sin \theta} \frac{\partial p}{\partial \phi} - \frac{\rho}{r \sin \theta} \frac{\partial \Phi}{\partial \phi} + f_\phi \end{aligned} \quad (4)$$

Here ρ denotes the density, p is the gas pressure and f_r, f_θ, f_ϕ are the viscous forces per unit volume in the radial, meridional and azimuthal directions, respectively. v_r, v_θ and v_ϕ denote the corresponding velocities. The gravitational potential Φ is given by

$$\begin{aligned} \Phi(\mathbf{r}) = & -\frac{GM_*}{r} - \sum_{p=1}^N \frac{Gm_p}{\sqrt{|\mathbf{r} - \mathbf{r}_p|^2 + \epsilon^2}} \\ & + \sum_{p=1}^N \frac{Gm_p}{r_p^3} \mathbf{r} \cdot \mathbf{r}_p + G \int_V \frac{dm(\mathbf{r})}{r^3} \mathbf{r} \cdot \mathbf{r}_p, \end{aligned} \quad (5)$$

where M_* is the stellar mass, ϵ is a softening parameter, and the summations are over all protoplanets p with masses m_p . The subscript ' p ' denotes evaluation at the location of the protoplanet. The latter two terms in Eq. 5 result from acceleration of the co-ordinate system due to the gravity of the protoplanets and the protostellar disc. The integral is performed over the volume of the disc.

Each protoplanet experiences the gravitational acceleration from the central star, the other protoplanets and the protostellar disc. The equation of motion for each protoplanet is:

$$\begin{aligned} \frac{d^2 \mathbf{r}_p}{dt^2} = & -\frac{GM_*}{r_p^3} \mathbf{r}_p - \sum_{p' \neq p}^N \frac{Gm_{p'}}{|\mathbf{r}_p - \mathbf{r}_{p'}|^3} (\mathbf{r}_p - \mathbf{r}_{p'}) \\ & -\nabla \Phi_d - \sum_{p'=1}^N \frac{Gm_{p'}}{r_{p'}^3} \mathbf{r}_{p'} \end{aligned} \quad (6)$$

where

$$\Phi_d(\mathbf{r}_p) = -G \int_V \frac{\rho(\mathbf{r}) d\mathbf{r}}{\sqrt{|\mathbf{r} - \mathbf{r}_p|^2 + \epsilon^2}} + G \int_V \frac{dm(\mathbf{r})}{r^3} \mathbf{r}_p \cdot \mathbf{r} \quad (7)$$

is the gravitational potential due to the disc. The integrals are again performed over the volume of the disc. The final terms in Eqs. 6 and 7 are the indirect terms arising from the acceleration of the coordinate system by the protoplanets and disc, respectively.

We adopt a locally isothermal equation of state such that the pressure and density are related by

$$p = c_s^2 \rho \quad (8)$$

where $c_s = \left(\frac{H}{r}\right) v_K$ is the isothermal sound speed, a fixed function of distance from the central star. v_K is the local Keplerian velocity. All disc models have aspect ratio $H/r = 0.05$. We also adopt the alpha model for the disc viscosity such that the kinematic viscosity $\nu = \alpha c_s H$, with $\alpha = 5 \times 10^{-3}$.

3. Numerical methods

We use two distinct numerical schemes: a 3D hydrodynamic disc model together with embedded planets is computed using a hydrodynamics code (NIRVANA); a suite of simulations are computed using a much faster N -body code which has been adapted to emulate the effects of orbital migration, and eccentricity and inclination damping on the protoplanets due to the protoplanetary disc. We describe each in turn in the following sections, and demonstrate that the modified N -body code agrees well with results from the hydrodynamic code.

3.1. Hydrodynamic scheme

We use a modified version of the grid-based code NIRVANA to conduct 3D hydrodynamical simulations (Zeigler & Yorke 1997). The code has previously been applied to a variety of disc-planet numerical studies in both two and three dimensions. Further details may be found in Nelson et al. (2000), Cresswell (2006), Cresswell et al. (2007) and in Paper I.

The motion of the protoplanets is integrated using a 5th-order Runge-Kutta scheme (Press et al. 1992). As in Paper I disc self-gravity is neglected. We employ reflecting boundary conditions in the meridional direction, and wave-damping conditions at the inner and outer radial boundaries. The implementation of these is described in Paper I, along with a description of the time step control procedure.

In common with many hydrodynamical disc simulations and Cresswell et al. (2007), we adopt a scale height $H/r = 0.05$ and surface density profile $\Sigma \propto r^{-0.5}$. A disc opening half-angle of 10° then models three and a half scale heights. Our adoption of a locally isothermal equation of state means that wave propagation is primarily confined to the radial direction, such that the use of reflecting boundary conditions at the meridional boundaries does not lead to significant wave reflection toward the disc midplane. The development of inclined orbits for the protoplanets, however, can cause the excitation of bending waves in the disc, which could in principle be affected by the vertical boundary conditions. Test simulations of inclined planets in discs using zero-gradient outflow boundary conditions, however, indicate that the results presented in this paper are not strongly affected by the choice of meridional boundary conditions. The adoption of reflecting conditions prevents the slow loss of mass from the disc which accompanies the use of open boundaries.

3.1.1. Code resolution and modelling

Due to the large computational expense of 3D disc-planet studies, the spatial resolution used in each model must be carefully weighed against the duration and number of simulations required. In Cresswell et al. (2007) it was found that the coarsest resolution tested produced results of a similar character in migration rate and eccentricity and inclination damping rates to the highest resolutions tested, with some difference in absolute migration/damping times; numerical convergence of the code was established with these high-resolution models. Since we have needed to run many simulations to obtain fitting formulae for the

modified N -body code, we have chosen a resolution for those simulations that leads to accurate results, but which makes the problem tractable: $(N_r, N_\theta, N_\phi) = (128, 40, 300)$. This resolution corresponds closely to the lower-resolution runs presented in Cresswell et al. (2007). The limits of the computational domain are defined by the intervals $r = [0.4, 2.5]$, $\theta = [80^\circ, 100^\circ]$, $\phi = [0, 2\pi]$. With the set-up described, we follow the evolution of a 10 Earth mass (M_\oplus) planet on a variety of eccentric and inclined orbits, and fit the migration and eccentricity and inclination damping rates using simple nonlinear functions of e and i .

We also performed one hydrodynamic simulation consisting of eight protoplanets embedded in a protoplanetary disc. The resolution adopted for this simulation was $(N_r, N_\theta, N_\phi) = (288, 40, 444)$, with the limits of the computational domain given by $r = [0.6, 3.0]$, $\theta = [80^\circ, 100^\circ]$, $\phi = [0, 2\pi]$.

3.2. N -body scheme

The second method we use to evolve a disc-planet system is an N -body integrator (to which we apply the name HENC-3D) with analytic functions which model the effects of type I migration, and eccentricity and inclination damping. The integrator used is the same 5th-order Runge-Kutta routine as used in NIRVANA. To prevent the time step from becoming too low, protoplanets were removed from the simulation if they fell within 10 Solar radii of the origin.

Due to the computational expense of 3D hydrodynamic computations, this is our primary method of evolving multiple-planet systems; even if it were practical to model a disc in NIRVANA over the scales required, HENC-3D is $\sim 10^7$ times faster at evolving such systems even at the moderate resolution we employ.

3.2.1. Prescriptions for eccentricity and inclination damping and migration

We construct prescriptions for the migration rates and eccentricity and inclination damping rates which are incorporated into the N -body code. These allow us to follow the evolution of protoplanet swarms for longer than is possible with the hydrodynamic code. Our starting point is the formulae for damping rates obtained by Tanaka & Ward (2004) and the migration rates obtained by Tanaka et al. (2002), which we modify using multiplicative factors that account for changes in damping and migration rates due to planetary eccentricity and/or inclination. These multiplicative factors are obtained by fitting formulae to the results of numerous hydrodynamical simulations, performed with different values of e and i . The results of a subset of these simulations are shown in Figs. 1–3. In the case of eccentricity and inclination damping, the formulae are founded on the damping time scale derived by Tanaka & Ward (2004), and given by their Eq. 49:

$$t_{\text{wave}} = \frac{M_*}{m_p} \frac{M_*}{\Sigma_p a_p^2} \left(\frac{H}{r}\right)^4 \Omega_p^{-1} \quad (9)$$

where $\Omega = v_\phi/r$ is the angular velocity of the unperturbed disc and Σ is the surface density

$$\Sigma = \int_{-\infty}^{\infty} \rho \, dz. \quad (10)$$

The eccentricity damping time that best fits our simulation results is given by:

$$t_e = \frac{t_{\text{wave}}}{0.780} \times \quad (11)$$

$$\left[1 - 0.14 \left(\frac{e}{H/r} \right)^2 + 0.06 \left(\frac{e}{H/r} \right)^3 + 0.18 \left(\frac{e}{H/r} \right) \left(\frac{i}{H/r} \right)^2 \right].$$

where the terms in square brackets provides the modification to the damping rate caused by the finite eccentricity and/or inclination. As was found by Papaloizou & Larwood (2000) and Cresswell et al. (2007), our results show that $de/dt \propto e^{-2}$ at high e , with exponential decay for $e < H/r$. The inclination damping time, t_i , is given by:

$$t_i = \frac{t_{\text{wave}}}{0.544} \times \left[1 - 0.30 \left(\frac{i}{H/r} \right)^2 + 0.24 \left(\frac{i}{H/r} \right)^3 + 0.14 \left(\frac{e}{H/r} \right)^2 \left(\frac{i}{H/r} \right) \right]. \quad (12)$$

where again the terms in square brackets modify the damping rate because of finite eccentricity and/or inclination. As described in Cresswell et al. (2007) we find $di/dt \propto i^{-2}$ at high i , with exponential decay for $i < H/r$.

The prescription for the migration time, t_m , is based on the results of Tanaka et al. (2002), who considered circular orbits only. The results of our simulations are well-fitted by the expression:

$$t_m = \frac{2t_{\text{wave}}}{2.7 + 1.1\beta} \left(\frac{H}{r} \right)^{-2} \left[P(e) + \frac{P(e)}{|P(e)|} \times \left\{ 0.070 \left(\frac{i}{H/r} \right) + 0.085 \left(\frac{i}{H/r} \right)^4 - 0.080 \left(\frac{e}{H/r} \right) \left(\frac{i}{H/r} \right)^2 \right\} \right] \quad (13)$$

where

$$P(e) = \frac{1 + \left(\frac{e}{2.25H/r} \right)^{1.2} + \left(\frac{e}{2.84H/r} \right)^6}{1 - \left(\frac{e}{2.02H/r} \right)^4}$$

and β is given by $\Sigma(r) \propto r^{-\beta}$. The sign dependency on $P(e)$ allows torque reversal at sufficiently high e . We note that Papaloizou & Larwood (2000) undertook a study of the disc-induced migration and eccentricity damping of low-mass protoplanets using linear theory, and derived similar expressions to those given in Eqs. 11 and 13. Our expressions differ from theirs only because we found that Eqs. 11 and 13 better fit our hydrodynamical simulations, and we consider both eccentric and inclined orbits.

We implement the following expressions in the N -body code as accelerations experienced by the protoplanets due to the disc, using values of t_m , t_e and t_i obtained from Eqs. 11–13:

$$\mathbf{a}_m = -\frac{\mathbf{v}}{t_m}, \quad (14)$$

$$\mathbf{a}_e = -2 \frac{(\mathbf{v} \cdot \mathbf{r}) \mathbf{r}}{r^2 t_e}, \quad (15)$$

$$\mathbf{a}_i = -\frac{v_z}{t_i} \mathbf{k}, \quad (16)$$

where \mathbf{k} is the unit vector in the z -direction.

3.2.2. Comparison between N -body and hydrodynamic code

We briefly demonstrate the agreement between the modified N -body and hydrodynamic codes. Figure 1 shows the orbital evolution of a planet on a variety of eccentric orbits, and the corresponding planetary migration. The decay of eccentricity at both

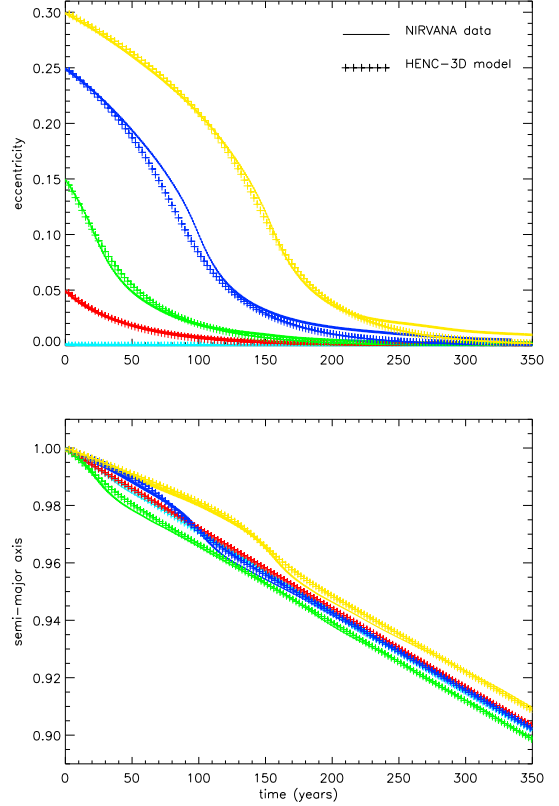


Fig. 1. (Top) Eccentricity evolution of a $10 M_{\oplus}$ protoplanet on a variety of eccentric orbits. Solid lines are the results from NIRVANA, crosses from the N -body code. (Bottom) The corresponding migration rates.

high and low eccentricity is modelled accurately, with the largest deviation at the transition from quadratic to exponential decay. We find that the exchange of angular momentum between disc and planet reverses sign when $e \gtrsim 2H/r$, rather than the value $e \gtrsim 1.1H/r$ reported by Papaloizou & Larwood (2000). In agreement with Cresswell et al. (2007), we find the peak positive angular momentum exchange rate (from the disc to the planet) to occur when $e \sim 4H/r$, rather than the value $e \sim 2H/r$ reported by Papaloizou & Larwood (2000). This may be an effect of adopting a different surface density profile.

Figure 2 shows the orbital evolution of a planet on a variety of inclined orbits, and the accompanying migration. As with the eccentric orbits, agreement between the hydrodynamic model and the modified N -body code is generally good, and poorest at the transition to exponential decay.

Figure 3 shows the orbital evolution of a planet on a variety of orbits which are both eccentric and inclined to the disc mid-plane. Agreement between the two numerical schemes is again good overall. The oscillations present in the most strongly excited runs are physical artefacts, and possess a frequency related to the precession rate of the longitude of ascending node. A bending distortion of the disc by the protoplanet is probably responsible, but does not significantly influence the underlying damping rate. It should be noted that our prescription for inclination evolution given by Eq. 12 does not include this oscillatory behaviour.

We note that it is not feasible to test planetary orbits with very high eccentricity or inclination against hydrodynamic mod-

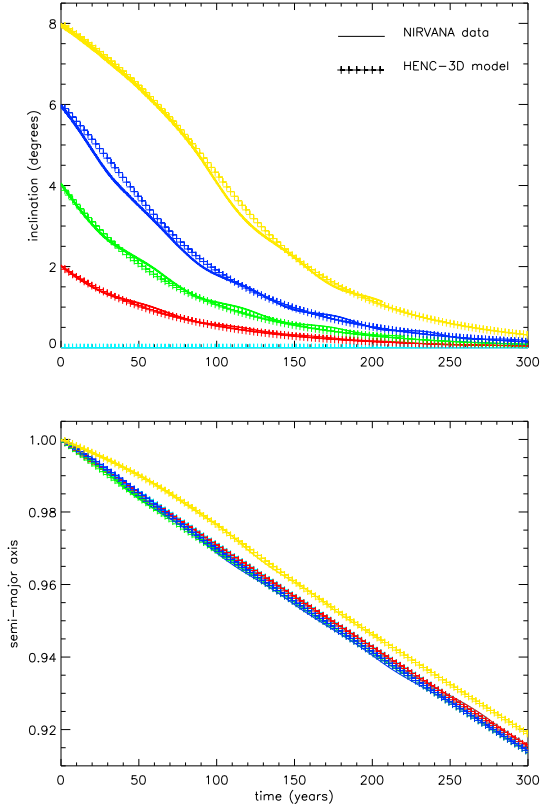


Fig. 2. (Top) Inclination evolution of a $10 M_{\oplus}$ protoplanet on a variety of inclined orbits. Solid lines are the results from NIRVANA, crosses from the N -body code. (Bottom) The corresponding migration rates.

els, due to the large range of scales over which the disc model must be simulated. However, previous experiments (Cresswell 2006) and Paper I imply that swarms of protoplanets will spend the majority of their time with fairly low eccentricities and inclinations. Equations 11–13 successfully capture the character of the dynamical evolution ($dy/dt \propto t$ at low y and $\propto y^{-2}$ at $y \gg H/r$, for $y = e$ or i) during the brief times when these quantities become large.

4. Initial conditions and units

We adopt a similar strategy to Paper I when setting up planetary initial conditions. We first define the semi-major axis of the innermost body to be $a_1 = 5$ AU, such that the population exists beyond the snow line where the proportion of solids available for protoplanet core formation is higher. Successive protoplanet semi-major axes were determined by choosing their separations to be a specified number of mutual Hill radii. Thus $a_{i+1} = a_i + N_{\text{mH}} R_{\text{mH}}$ where N_{mH} is typically 5 (though other values are considered). The mutual Hill radius is defined by

$$R_{\text{mH}} = \left(\frac{m_i + m_j}{3M_*} \right)^{\frac{1}{3}} \left(\frac{a_i + a_j}{2} \right). \quad (17)$$

For two planets on initially circular orbits, rapid instability occurs if the separation Δ between planets is less than the critical value

$$\frac{\Delta_{\text{crit}}}{R_{\text{mH}}} = 2\sqrt{3} \approx 3.46 \quad (18)$$

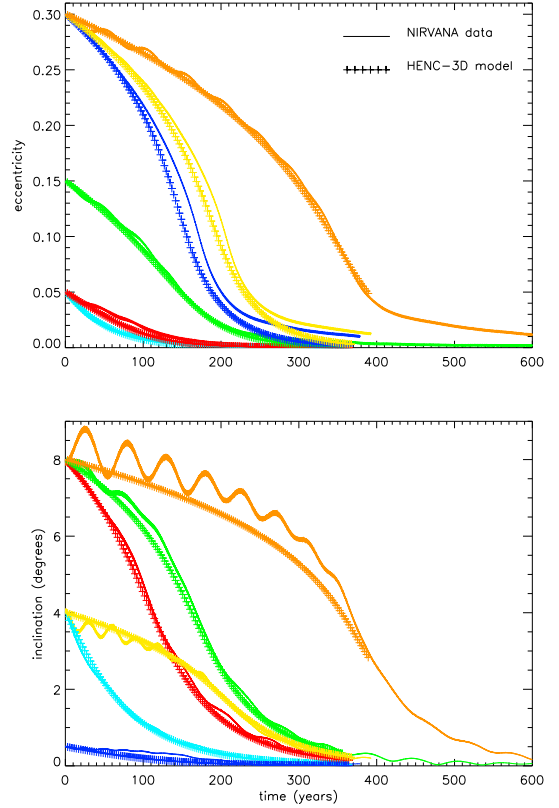


Fig. 3. (Top) Eccentricity evolution of a $10 M_{\oplus}$ protoplanet on a variety of eccentric and inclined orbits. Solid lines are the results from NIRVANA, crosses from the N -body code. (Bottom) Inclination evolution of the same orbits.

(Gladman 1993; Chambers et al. 1996). Simulations of oligarchic growth (Kokubo & Ida 2000; Thommes et al. 2003) suggest that the mutual separation of protoplanets is normally $\approx 8 R_{\text{mH}}$. We typically adopt smaller spacings to maximise close encounters, although larger separations are also investigated.

Planetary eccentricities were determined by defining a mean eccentricity μ_e for the planetary swarm, and standard deviation $\sigma_e = 0.01$, with eccentricities then chosen randomly according to a Gaussian distribution. Each body is given a random argument of pericentre. Inclinations are likewise Gaussian distributed according a mean $\mu_i = 0^\circ$ and standard deviation σ_i , with random longitude of ascending node.

Two different schemes were used to determine initial planetary masses. In the ‘ordered’ models, the standard procedure was to define the mass of the innermost body (usually $m_1 = 2 M_{\oplus}$) with subsequent bodies having $m_{i+1} = m_i + 2 M_{\oplus}$. This somewhat artificial set-up was chosen to maximise convergent migration, and hence maximise interactions between the bodies. In the ‘randomised’ models, a more natural distribution is formed from a randomly selected Gaussian distribution of planetary masses, with mean μ_m and standard deviation σ_m , subject to a lower-mass cutoff of either 2 or $0.2 M_{\oplus}$, and an upper cutoff of $20 M_{\oplus}$ (but note that collisions may raise masses above this value).

The disc was initialised with scale height $H/r = 0.05$ and $\Sigma(r) = \Sigma_0 r^{-0.5}$, where Σ_0 was typically chosen such that the disc contains 40 Jupiter masses of gaseous material within 40 AU of the central star. Other disc masses and surface density

Set	μ_e	σ_i	μ_m	σ_m	Cutoff	Δ_0	Σ	N_p
H1	0.05	2°	-	-	-	5	1	8
O1	0.05	2°	-	-	-	5	1	10
O2	0.15	2°	-	-	-	5	1	10
O3	0.05	6°	-	-	-	5	1	10
O4	0.10	4°	-	-	-	5	1	10
O5	0.05	2°	-	-	-	4	1	10
O6	0.05	2°	-	-	-	8	1	10
O7	0.05	2°	-	-	-	5	0.5	10
O8	0.05	2°	-	-	-	5	0.2	10
O9	0.05	2°	-	-	-	5	1	5
R1	0.05	2°	10	7	0.2	5	1	10
R2	0.05	2°	10	5	2	5	1	10
R3	0.05	2°	10	3	2	5	1	10
R4	0.05	2°	7	3	2	5	1	10
R5	0.05	2°	7	5	0.2	5	1	10
R6	0.10	2°	10	5	2	5	1	10
R7	0.05	4°	10	5	2	5	1	10
R8	0.10	4°	10	5	2	5	1	10
R9	0.05	2°	10	5	2	4	1	10
R10	0.05	2°	10	7	0.2	6	1	10
R11	0.05	2°	5	3	0.2	8	1	10

Table 1. A subset of the 3D models performed. From left to right, the columns give: class name; mean eccentricity; standard deviation of inclination; mean mass; standard deviation of mass; lower-mass cutoff; initial separations in mutual Hill radii; disc mass (normalised against fiducial value); number of protoplanets.

profiles were also used, and are described where appropriate in subsequent sections of this paper. In the NIRVANA simulation the disc had a viscous alpha parameter of $\alpha = 5 \times 10^{-3}$ (Shakura & Sunyaev 1973).

The distribution of semi-major axes, planet and disc masses, and values of μ_e , σ_e and σ_i together define a class of model. For each model class five realisations of the initial data were generated by rotating the random number seeds, giving rise to five different simulations. In total over 300 simulations were run; details of a subset of the models used are given in table 1, including those described in subsequent sections.

5. Results of the hydrodynamic simulation

One 3D hydrodynamic run (case H1) was performed to complement the N -body models. We adopted the fiducial ordered mass set-up, to maximise convergent differential migration. To model the system for over 2×10^4 years while preserving the grid resolution, eight protoplanets were used so that the radial extent of the grid could be lessened (ten protoplanets were normally used in the N -body simulations described later). The protoplanets take the same masses as the eight inner bodies of the fiducial ordered runs, so that the inner body is $2 M_\oplus$ and the outer is $16 M_\oplus$. The number of active cells used was $(N_r, N_\theta, N_\phi) = (288, 40, 444)$; this provides a resolution finer than those used to construct Eqns. 11–13 by a factor of 1.5 in azimuth and 2 in radius. As in those tests, for the potential softening we adopt a value almost one tenth the vertical height of a cell.

The results of this model are shown in Fig. 4. Resonant migration dominates the model: after a short period of low-level scattering and orbital exchanges (where horseshoe interactions rearrange the radial ordering of two adjacent protoplanets), the system settled down into two groups of planets which are in mu-

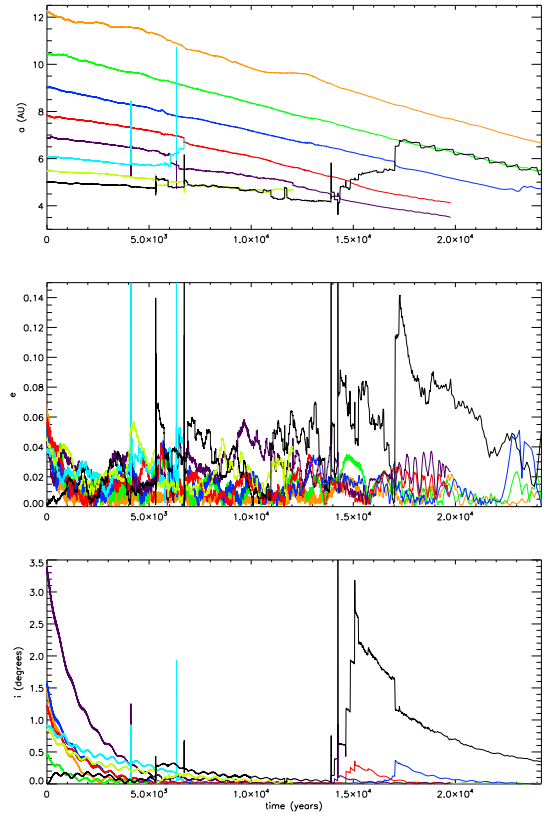


Fig. 4. Orbital elements for the 3D NIRVANA model, similar to Fig. 5 but with eight protoplanets (run H1). Behaviour is similar to the early stages of the N -body models, with scattering and collisions among the inner population. A co-orbital system is formed, which remains stable for the remainder of the integrations. Note only the smallest protoplanet achieves $e > 0.1$ or $i > 0.5^\circ$ after the initial values have been damped. The 6 & 10 M_\oplus protoplanets collide at $t = 6.7 \times 10^3$ yrs, and the 4 & 8 M_\oplus protoplanets collide at $t = 1.20 \times 10^4$ yrs.

tual mean-motion resonances, with all resonances being either 4:3 or 5:4. The inner pair have suffered collisions (at 6.7×10^3 and 1.2×10^4 yrs) and end the scattering phase in a 5:4 MMR and on orbits diverging from the external protoplanets due to their increased mass; they are no longer plotted once the inner body of the pair enters the inner damping region, but based on all other models performed, we expect this pair would continue to migrate inward in resonance.

Resonant migration is thus the dominant outcome of the simulation. Only the smallest, scattered body achieves a significant eccentricity or inclination, with the other protoplanets limited to $e < 0.1$ and $i < 0.5^\circ$ once their initial values have been damped by the disc. By the end of the run all other protoplanet inclinations are near zero due to the strong damping. In the absence of a magnetospheric cavity, or other halting mechanism, we expect all protoplanets to migrate into the central star.

One further point of note is that a co-orbital pair of planets are observed. Initially this involves the planets undergoing mutual horseshoe motions, but it is expected from the results of Paper I that the damping action of the disc will reduce the libration width until tadpole orbits result. The co-orbital pair remains stable in simultaneous resonant migration with other bodies on

both interior and exterior orbits for the remainder of the integration.

Despite a total run time of over 1.5×10^5 cpu hours on a parallel facility, due to the high cost of performing hydrodynamic simulations in three dimensions we are unable to continue this simulation for more than a few $\times 10^4$ years, nor repeat other similar simulations many times in order to gain a statistical overview of these chaotic systems. Instead, we perform numerous N -body simulations using the HENC-3D code to examine these issues.

6. Results of the modified N -body simulations

We have performed more than 300 modified N -body simulations to examine the evolution of clusters of low-mass protoplanets embedded in a 3D protoplanetary disc, varying planet masses, orbital parameters, and disc masses. Despite all this variation in initial conditions, a number of simple trends are observed. We present a select few results to illustrate these trends. Further detail of the 2D analogues of these trends may be found in Paper I.

6.1. A fiducial ordered mass N -body simulation

We choose one particular class of model (class O1 in table 1) to act as the fiducial case, against which other models are compared. As shown in Fig. 5 the model follows a typical pattern: differential migration initially causes the planets to move closer to each other. In the outer half of the swarm, orbital exchanges, where two planets appear to swap semi-major axes in a horse-shoe motion, may occur. A similar situation is seen among the inner half; however, due to the larger mass ratios m_{i+1}/m_i between neighbouring inner bodies such an exchange leaves the less massive planet with a slightly larger semi-major axis than the body it has just replaced, according to the simple ratio $\Delta a_j/\Delta a_i \approx m_j/m_i$. The smaller body is now closer to the next external mass than the previous planet was, making further such exchanges (themselves with larger m_j/m_i) more likely. In this manner the smallest masses in the population are often passed outward from planet to planet, gaining in eccentricity and inclination in the process. This process typically culminates with: (i) collision with another body; (ii) co-orbital capture; (iii) ejection beyond the outer edge of the swarm. A rarer fourth outcome is capture in the Hill sphere of another body, forming a planet-moon or binary planet system. HENC-3D is not equipped to model such encounters accurately, which always result in a collision after a few $\times 10^4$ years. The process may repeat for several of the smallest bodies, such that the initially innermost planets finally constitute (in some ordering) the outermost planets of the swarm, with the original outermost bodies now leading the inward migration having ‘pushed through’ the swarm.

As the population of planets converges due to differential migration, a series of mean-motion resonances (MMRs) forms between the planets (or subsets of them), forcing them to migrate inward in lockstep. Occasional bursts of dynamical instability occur, leading to the removal of bodies by collision, co-orbital capture or ejection to the outer edge of the swarm, and this helps stabilise the population. The initial phase of scattering smaller bodies ends within a few thousand years, and the disc rapidly damps eccentricities and inclinations developed during this active phase. During the ensuing resonant migration, as separations between the planets decrease, a single planet is occasionally perturbed sufficiently to break the resonant chain, and the process of the swarm reordering itself may repeat on a shorter time scale (often $< 10^3$ yrs), as seen in Fig. 5 at time $t \approx 6.5 \times 10^5$

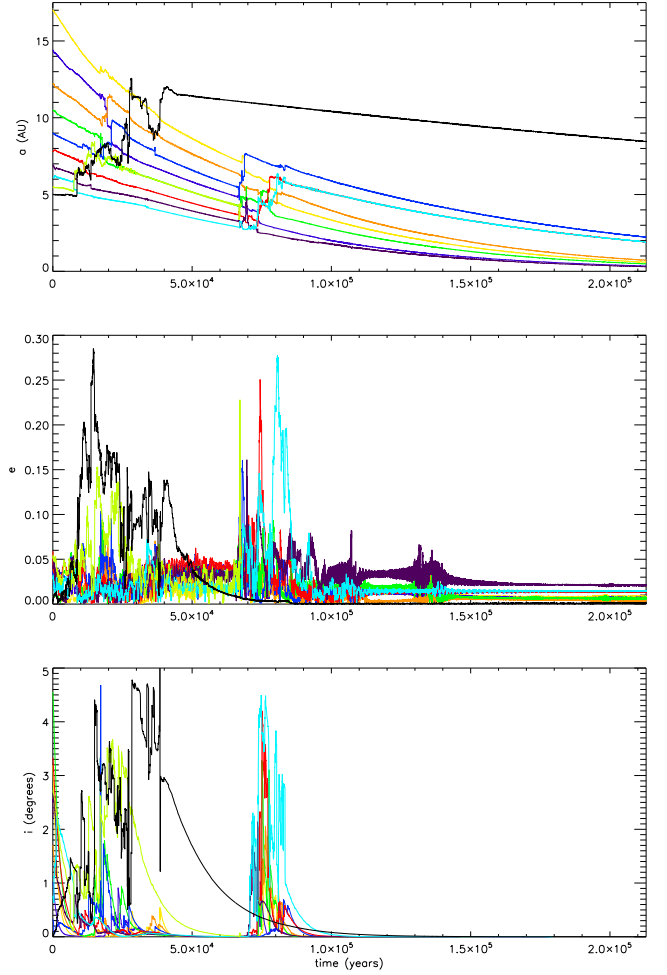


Fig. 5. Evolution of a 10 planet N -body model with ordered masses and the fiducial set-up (O1). (Top) Semi-major axes of the migrating embryos. Short periods of activity are followed by long periods of migration between bodies in first order mean-motion resonances. The 4 & 18 M_{\oplus} planets collide at $t = 6.76 \times 10^4$ yrs. (Middle) The embryos’ eccentricities over the same time. (Bottom) The embryos’ inclinations.

years. Ultimately the population, now comprised of an individual planet and two resonant groups, migrates towards the central star, where it will be accreted in the absence of a stopping mechanism, such as a disc edge created by a magnetospheric cavity, or a ‘planet trap’ associated with a region of the disc with a positive surface density gradient (Masset et al. 2006). The final masses of the planets, labelled from smaller to larger radii at the end of the simulation, are (first group) 8, 22, 14, 20, 16 M_{\oplus} , (second group, including the co-orbital pair) 10, 6, 12 M_{\oplus} , and 2 M_{\oplus} , showing how the population has separated with the smallest bodies at larger radii and the largest bodies closer to the star. The smallest planets, if scattered significantly far outwards, or with sufficient eccentricity or inclination to slow their migration, may survive for times on the order of 10^6 years, raising the possibility of survival as a super-terrestrial body if the population formed late in the disc’s lifetime.

Due to the strong inclination damping, the system is approximately planar for most of its duration. As the planets migrate together, the MMRs between neighbouring bodies are almost al-

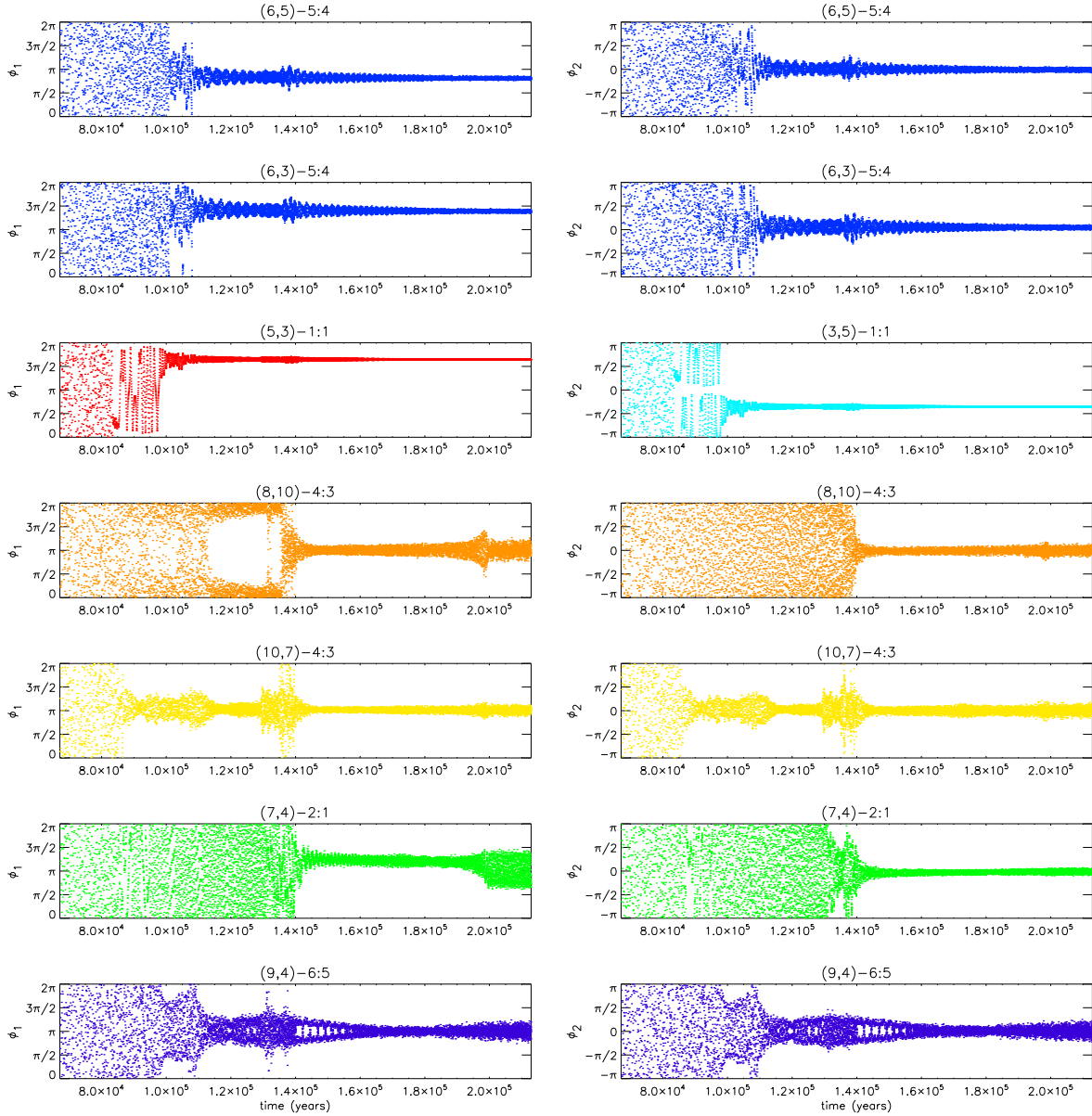


Fig. 6. The first order mean-motion resonances between the planets in Fig. 5, during the longest resonant migration phase. Each plot is labelled $(P_i, P_j) - p:q$, where P_i and P_j are the exterior and interior protoplanets in each resonance respectively, and $p:q$ is the commensurability between them.

ways ($> 99\%$) first order, typically 3:2, 4:3, ..., 8:7. The first order and co-orbital resonances between the planets in Fig. 5 are shown in Fig. 6, where the planets are labelled 1–10 with 1 being the initially innermost body, and 10 the initially outermost. The resonant angles for the first order resonances ($p = q + 1$) are defined by:

$$\begin{aligned}\phi_1 &= p\lambda_1 - q\lambda_2 - \omega_1 \\ \phi_2 &= p\lambda_1 - q\lambda_2 - \omega_2\end{aligned}\quad (19)$$

where λ_1 (λ_2) and ω_1 (ω_2) are the mean longitude and longitude of pericentre for the outer (inner) planet, respectively. Commonly, the complicated lattice of resonances between groups of planets generates additional first, second and third order resonances between non-neighbouring planets (*e.g.* alternating 5:4 and 6:5 resonances implies the existence of a 3:2 resonance between the non-neighbouring planets). Rather than being

a source of perturbation to resonant pairs, additional planets thus often provide further stability to a migrating resonant group.

In Sect. 6.5 we present a more statistical analysis of our results, but in the next subsection we discuss how the qualitative nature of the results change as initial conditions are varied.

6.2. Variation of the initial conditions

The behaviour discussed above represents the typical behaviour observed among the ordered mass models. Many other sets of initial conditions were used, including varying initial eccentricities and inclinations up to $\mu_e = 0.15$ and $\sigma_i = 6^\circ$ (*e.g.* runs O2–O4).

6.2.1. Variation of initial eccentricities

Increasing the initial eccentricities typically produces a much longer dynamically active phase among the swarm, which involves more planets and prevents the formation of early but temporary resonant groups. This is especially true when the initial eccentricities are such that protoplanets begin on crossing orbits. Much of the population is involved in dynamical relaxation until several bodies have been expelled from the group, or lost in collisions. In the long run, however, the final states of these systems are similar, and consist of inwardly migrating groups of planets, in multiple mean-motion resonances, often including co-orbital systems. Their final fate remains accretion by the central star.

6.2.2. Variation of initial inclinations

Raising initial inclinations has little effect, as they are damped by the disc before large-scale scattering activity begins. This is to be expected as raising inclinations does not lead to the creation of crossing orbits, unlike the initial eccentricity variations. Systems with large values of initial inclination have their inclinations damped on the time scale of a few thousand orbits, after which they enter a phase of dynamical interaction similar to that shown by the fiducial run described in Sect. 6.1.

Scattering throughout the population is now more common overall than in 2D (see Sect. 6.5) and the resulting activity largely removes memory of the initial conditions. For the initial eccentricity/inclination distribution to substantially alter the long term evolution requires seemingly unphysical values for these quantities, corresponding to non-disc-like initial conditions.

6.2.3. Variation of initial separations

The initial separations between the planets were varied, with values ranging between 4 and 8 R_{mH} . This was found to have no qualitative effect on the final states of the systems. Early stages showed significant differences, with closer protoplanets undergoing prolonged periods of violent excitation, and more distant ones slowly moving closer together and taking longer to produce any significant scattering activity. Once scattering activity ceased to continue the final states of the systems were again very similar to those already described.

6.2.4. Modifying the disc mass

Altering the disc mass produced more substantial changes. Reduction by a factor of 2 (class O7) produced population-wide gravitational interactions for similar lengths of time ($\sim 1\text{--}2 \times 10^5$ years) despite longer migration times, yet the swarm was more likely to retain its original order, with fewer of the more massive planets passing through the population and instead remaining at the rear of the population where they drive the whole group forward. This presumably arises because of the overall reduction in convergent migration rates. The resonant groups were often larger, comparable to those seen in 2D (consisting of up to 7 bodies). However, those small planets that were scattered tended to achieve higher eccentricities ($e \approx 0.5\text{--}0.6$) and higher inclinations ($6^\circ\text{--}12^\circ$), and remained in such excited orbits for several times longer than in the fiducial case. By spending significant portions of each orbit away from the other protoplanets (due to the high inclinations), encounters that may result in collisions or co-orbital pairs become less likely, allowing the smaller body to retain its excited state for longer. Further reductions in disc

mass increased the effect slightly and were more likely to produce larger resonant groups.

6.2.5. Changing the number of planets

We have run models with smaller numbers of protoplanets (five rather than ten). One such model is listed as class O9 in table 1. Although the early phase of evolution can occasionally involve all planets being in mutual mean-motion resonances, this configuration was found to be stable for long time scales in only approx. 20% of runs; interestingly, only those models that formed a stable co-orbital pair were able to sustain such a five-planet resonant group. In all other cases instabilities leading to scattering reduced the group size, either by ejecting one of the smallest protoplanets to a larger orbit (most common when the initial mass range of protoplanets was largest, $2\text{--}20 M_\oplus$) or by removing one or more protoplanets by collision (most common when the initial mass range was smallest, $2\text{--}10 M_\oplus$). In all cases the long-term evolution always resulted in migration of the remaining protoplanetary swarm into the central star.

6.3. A fiducial randomised mass N -body simulation

When initiating models with randomised masses, we set a mean μ_m and standard deviation σ_m for the mass distribution, and chose masses randomly according to a Gaussian distribution. A wide range of mass distributions were considered, which were conflated with the variations in initial conditions used in the ordered mass models. For a fiducial randomised model, we choose initial conditions and the planetary mass range similar to the fiducial ordered case (class R1). Such a model is shown in Fig. 7.

Overall, randomised models follow broadly similar evolutionary paths to the ordered models, except that differential migration carries some planets, or groups of planets, away from each other. Consequently, unless the early gravitational interactions among the population are prolonged or involve especially strong scattering, the protoplanets rapidly ($< 5 \times 10^4$ yrs) break up into smaller groups of typically 2–5 bodies, with the slowest migrators typically following behind in isolation after scattering. This behaviour is clearly seen in Fig. 7 and also in Fig. 8, which shows snapshots of the end-states of a random selection of models. Planets of the largest or smallest mass typically end the simulation migrating alone or in small groups at the inner or outer edges of the population, respectively.

6.3.1. Variation of the mass distribution

Several different mass distributions were combined with the various initial eccentricity and inclination distributions that we have considered previously. Values in the range $5 M_\oplus < \mu_m < 10 M_\oplus$ and $3 M_\oplus < \sigma_m < 7 M_\oplus$ (e.g. classes R1–R5) were used in setting up initial protoplanetary swarms. The resulting models can be characterised by a number of features.

First it was found that among the primary mass ranges studied ($5 \leq \mu_m \leq 10 M_\oplus$), when $\sigma_m \lesssim \mu_m/3$ scattering was substantially reduced, resulting typically in one large group migrating without further strong interaction after an initial period of orbital readjustment. This is clearly due to the fact that the planets are migrating inward at similar rates. For larger ratios of σ_m/μ_m planet-planet scattering and its natural consequences (collisions, co-orbital planets, etc.) were more common, due to the concomitant increase in differential migration. Once strong scattering

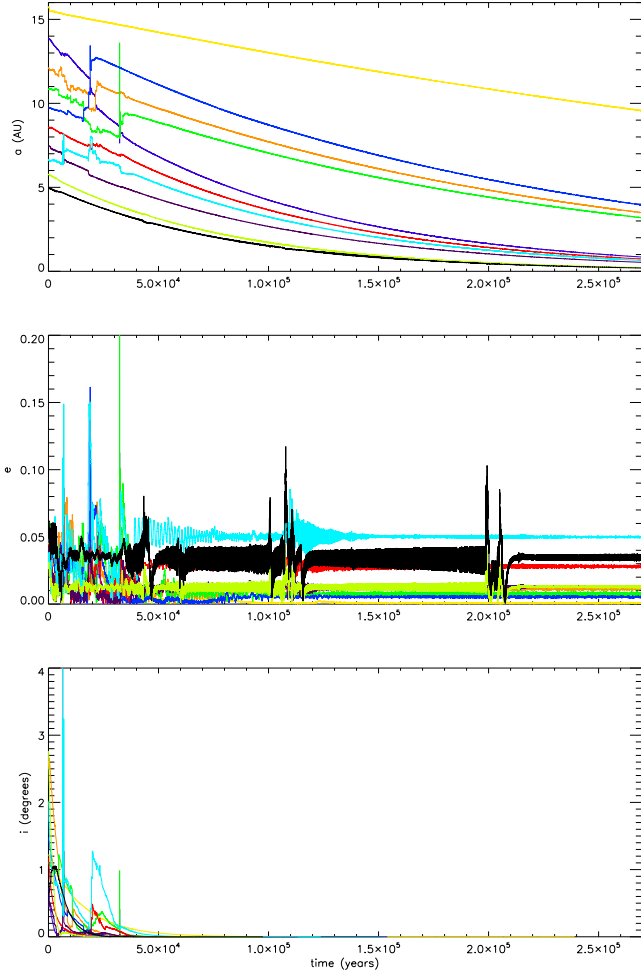


Fig. 7. Evolution of a 10 planet N -body model with randomised masses and the fiducial set-up (R1). (*Top*) Semi-major axes of the migrating embryos. Short periods of activity are followed by long periods of migration of bodies in first order mean-motion resonances. (*Middle*) The embryos’ eccentricities over the same time. (*Bottom*) The embryos’ inclinations.

was induced, however, we found no strong correlations between the final outcomes and the value of σ_m/μ_m .

The second feature we note is that additional tests for lower-mass planets (see Sect. 6.4.1 for a more complete discussion), using mean masses in the interval ($0.3 \lesssim \mu_m \lesssim 2 M_\oplus$), seem to result in more energetic and population-wide scattering activity than is the case for higher-mass planets, which may seem surprising at first glance. This result appears to originate in the fact that the lower-mass planets tend to become trapped in first order resonances of high degree (even as large as 14:13 for the lowest mass cases considered), placing the planets in very close proximity. Localised instabilities in the resonantly migrating swarm then lead to strong dynamical interaction and scattering. Such large-scale activity was also seen among ordered mass runs using similarly small initial masses.

The third feature shown by the randomised mass runs is that the initial distribution in semi-major axes of the bodies determines much of the subsequent evolution. If the innermost bodies are of a higher mass than the mean of the population, those planets will form a separate group and migrate away from the rest,

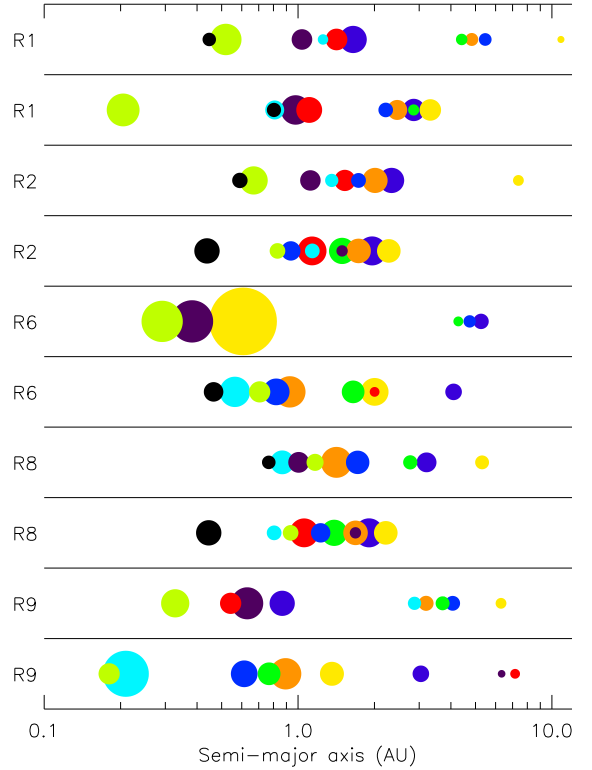


Fig. 8. Snapshots of two randomly selected simulations from the model classes shown, with the exception of the first (R1) and fourth (R2) rows, which correspond to Figs. 7 & 9 respectively. The snapshots are taken at $t = 2 \times 10^5$ yrs. The area of each planet is linearly proportional to its mass; the smallest body (in the top row) is of $2 M_\oplus$, and the largest (formed from multiple collisions) is of $39 M_\oplus$. The co-orbitals of Fig. 9 are clearly visible as concentric circles.

generally leading to an uneventful inward journey for the whole population. Conversely, if several massive bodies are located in the outer half of the population, then they are likely to drive a larger resonant group ahead of themselves, usually causing the smallest bodies to be scattered outwards, and also more likely to generate co-orbital systems.

The fourth feature we observe is that the initial distribution of masses has more effect on the resulting level of activity than their initial separations. That is, although it may take longer for differential migration to bring together initially widely separated bodies, the resulting activity is determined by the mass distribution just as it is when the protoplanets are initially closer together. Separations of up to $20 R_{\text{MH}}$ have been tested, with the mass distribution remaining the dominant factor.

Together, these features suggests that the level of activity among a population of moderate to large cores, assuming a moderate spacing of several mutual Hill radii, is dependent on the mass ratios of nearby bodies, with little scattering activity below a critical value $\sigma_m/\mu_m \lesssim 1/3$ for a Gaussian distribution. Collections of smaller masses appear to undergo periods of evolution where the degree of scattering activity is greater than for their more massive counterparts. We note that the smaller protoplanets generally form MMRs of higher degree, in the range 8:7–10:9 (or in more extreme cases 14:13), which in conjunction with the weaker damping forces on eccentricity and incli-

nation may account for the increased scattering due to closer proximity. Nonetheless, we observed that in some cases these resonances could remain stable over long periods, and examples of long term stable planets in the 14:13 resonance occurred in some simulations.

Varying the mass distribution produced no significant correlation with any other parameter variation (Sect. 6.2).

6.4. Prevalence of co-orbital systems

A significant feature that arose in Paper I was the unexpected abundance of stable co-orbital planets, orbiting around their mutual L_4/L_5 points. Co-orbital systems form when planet-planet scattering causes a planet to be perturbed such that its semi-major axis becomes very similar to that of another planet in the system. Disc-induced eccentricity damping then ensures rapid decay of the planet eccentricity, leading to co-orbital capture. Within the planetary swarm, the condition for long-term capture is simply that this eccentricity decay occurs before the scattered planet undergoes a close encounter with another protoplanet, which would otherwise disrupt the co-orbital system. We find that many of the co-orbital systems remain stable for the duration of the simulation while migrating inward over distances greater than 10 AU.

In 3D, we find that these co-orbital planets are more common than in 2D (see Fig. 10), occurring in almost 45% of ordered and almost 35% of randomised simulations; of these, approximately 21% and 14% respectively contained multiple examples of stable, co-orbital pairs in the same simulation (as with other resonances, co-orbital pairs are deemed stable within a simulation if they survive for a time $> 10^5$ years.) We note that the eccentricity damping rate adopted in the 2D simulations of Paper I was smaller than that used for the 3D runs in this paper. We attribute this increased co-orbital frequency to the higher eccentricity damping rate and the generally smaller sizes of the resonant groups — both of which reduce the opportunity for a recently captured co-orbital body to be disturbed by other protoplanets — together with a slight increase in overall scattering activity (Sect. 6.5). Inclined orbits are not an obstacle to co-orbital formation, and planets with inclinations greater than 10° are readily captured into stable horseshoe orbits, with these mutual inclinations eventually being damped by the disc.

When a co-orbital system first forms it is usually in a mutual horseshoe orbit. In all except one instance the horseshoe motions decayed because of the disc's action to form tadpole orbits, maintaining small oscillations about the L_4/L_5 points. The transition from horseshoe to tadpole motion typically takes $0.3\text{--}1 \times 10^4$ years for our standard disc parameters.

A detail of two migrating co-orbital systems (from class R2) is shown in Fig. 9. Initially the horseshoe librations are of large amplitude, but these decrease with time, and after $2\text{--}3 \times 10^3$ yrs tadpole motions result. The system then continues to migrate inward maintaining this architecture.

Co-orbital planets are found both as isolated pairs, and as part of larger resonant groups, sharing mean-motion resonances with external and internal bodies like any other individual body. At the end-state of a simulation, a co-orbital pair may thus be in multiple first- and second-order MMRs with two or more interior/exterior bodies, all densely packed within 0.4 AU of the star.

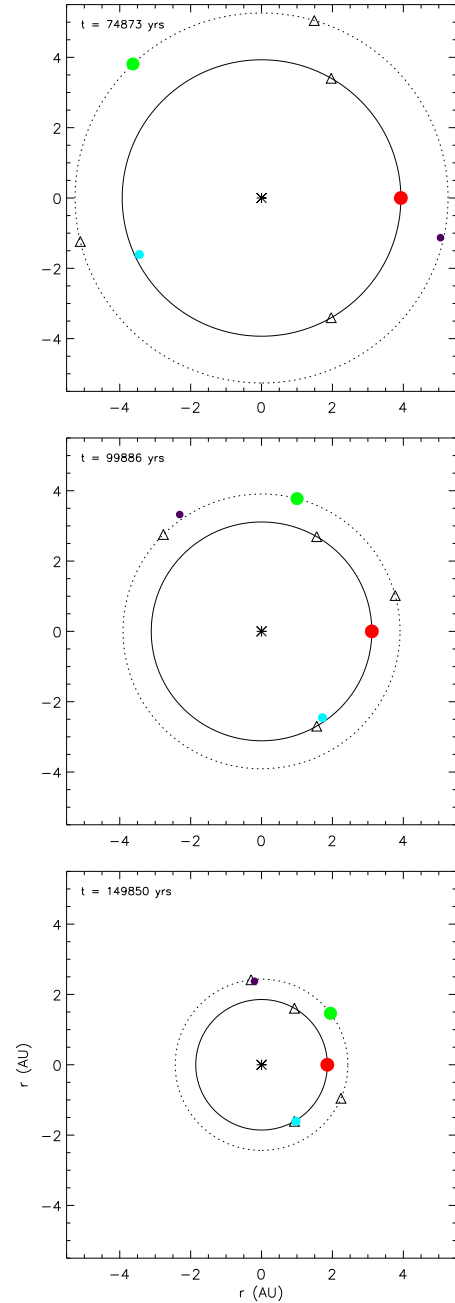


Fig. 9. Evolution of a co-orbital system (class R2) migrating inwards: two co-orbital pairs, locked in a 3:2 MMR. The size of each planet is proportional to its mass, while the open triangles display each primary body's L_4 & L_5 points. The other protoplanets present in the model are not displayed, but those shown are part of a resonant group encompassing nine bodies. (Top) Initially the co-orbital planets' motions cover the whole horseshoe region. (Middle) The disc's action causes the planets to shift into tadpole orbits. (Bottom) The planets migrate inwards under small librations.

6.4.1. Limits on co-orbital formation

Other studies have examined the behaviour of swarms of protoplanets, subject to type I migration, at earlier stages of formation when protoplanetary masses are considerably smaller (e.g. McNeil et al. 2005). Similar patterns of resonant migration have been observed, but co-orbital planets were not found, in

contrast to their ubiquity here and in Paper I. Consequently, we seek to determine limits on co-orbital formation and explain this discrepancy between models; we focus on planetary mass, initial separations, and the surface density profile of the disc.

To compare with studies conducted using lower-mass protoplanetary swarms, we selected one fiducial class from each of the ordered (O1) and randomised (R1) models, and reran them with the protoplanets' masses (μ_m and σ_m , in the randomised case) repeatedly halved; the lower-mass cut-offs are set to 0 in both cases (see Sect. 6.3.1). Additionally, in the randomised models we increased the initial separations in stages up to $20 R_{\text{mH}}$.

When using our standard disc model with these smaller protoplanet masses, 25% of simulations resulted in stable co-orbital pairs for both the ordered and randomised mass distributions, averaged over the ranges of planetary masses and initial separations considered.

With smaller sample sizes, we can be less confident about these statistics than for the main body of the simulations performed. However, the fact that co-orbitals continue to appear at all, and with frequencies of $\sim 25\%$, is significant. The region within which co-orbital capture can occur scales $\sim m_p^{1/3}$, and so we may expect capture rates to fall to near zero for populations of such small bodies. However, differential migration brings protoplanets closer together; as masses decrease, the MMRs formed between neighbouring protoplanets are of higher degree (stable resonances up to 14:13 were observed among this work, as mentioned previously) and so the planets lie closer together. Consequently only a small shift in the orbit is necessary for one body to enter the horseshoe region of another and be captured, and a perturbation from a third body can provide the necessary energy to jump into the horseshoe region. All that is required for co-orbital formation is 3–4 protoplanets in close proximity.

We also note that, for the randomised mass distributions, co-orbital frequency is essentially independent of the initial separations. This is easily interpreted as resonant migration driving groups of bodies together; differential migration may cause a relatively massive protoplanet to 'sweep up' several smaller bodies in MMRs ahead of it. Formation of a co-orbital pair from such collections is then dependent only on the usual mutual interactions within a small group. Provided the initial separations are not so large that such groups do not have time to form — highly unlikely for most oligarchic growth scenarios, *e.g.* Kokubo & Ida (2000) — co-orbital formation thus remains primarily dependent on the initial mass distribution.

One feature different here from the set-up of McNeil et al. (2005) are the disc damping times, where they utilised the higher damping rates of Papaloizou & Larwood (2000); the discrepancy is approximately given by a factor of 3 (see also Figs. 1 & 2 of Paper I). To test the effect of this difference, we shortened the damping time in Eqn. 11 by this factor, and reran a selection of models with the lowest mass distributions previously considered. We find that although interactions between the planets are significantly reduced, co-orbital planets are still able to form as differential migration brings a population together, with crowding producing the minor perturbations and individual orbital exchanges required, despite low eccentricities among the group.

The situation changes dramatically when the disc surface density profile is steepened. We ran a suite of models with the power law exponent being decreased to $-3/2$, which is the value usually adopted for the minimum mass solar nebula (Hayashi 1981), and corresponds to the disc model used in McNeil et al (2005). In this case the incidence of co-orbital system formation fell to almost zero, this being a direct consequence of the fact that the migration of interior bodies is speeded up, and that

of bodies lying further out in the disc is slowed down, when the density profile is steepened. Thus, it would appear that co-orbital planet formation is highly sensitive to there being strong differential migration that brings bodies together, a situation that is highly favoured in discs with flatter surface density profiles. Observation of co-orbital extrasolar planets would thus be an indicator of strong dynamical relaxation occurring during planet formation, induced and maintained in-part by there having been a suitably flat radial surface density profile in the original protoplanetary disc.

6.4.2. Long-term stability

To test the stability of these tadpole planets during and beyond disc dispersal, a time-dependent function was added to Eq. 9 that reduced the disc-induced forces acting on the planets exponentially, simulating disc mass loss according to a prescribed time scale. We then selected several simulations that produced tadpole planets, removed the other planets, and restarted the model after the formation of the co-orbital pair. Each pair was found to separate if the disc forces were reduced too rapidly, typically corresponding to a (grossly unphysical) mass-halving time of under 10^5 years. In all other cases, the co-orbital pair remained stable, with their orbits remaining largely unchanged once the remaining simulated disc mass became negligible.

Test calculations were also run in which the non-co-orbital planets were not removed from the system, and these contained instances where: the co-orbital pair was largely isolated from all other bodies because of prior differential migration; the co-orbital pair were on significantly eccentric orbits (both planets possessing $e > 0.25$); the co-orbital pair were in resonance with additional bodies driving faster inward migration (while the migration force remained effective). Subject to the condition on disc mass-halving time stated above, all these models were found to be stable for as long as the integrations were continued, with a minimum simulation time of $\sim 2 \times 10^5$ years in each case and a typical duration an order of magnitude greater. One model was allowed to evolve in a disc-free environment for over 4×10^9 years, with the co-orbital system remaining stable for this time.

We note those models with additional planets in mean-motion resonance with the co-orbital pair also implies the long term stability of pairs of protoplanets in MMR after disc dispersal, and these resonant systems often contain numerous bodies in mutual MMRs. While the observed exoplanets in MMR are giant planets (*e.g.* GJ 876, 55 Cancri, HD 128311, HD 82943, HD 7352), whose resonances are thought to have been established through differential type II migration (*e.g.* Snellgrove et al. 2001; Lee & Peale 2002; Kley et al. 2004), our simulations show that differential type I migration may lead to the formation of multiple MMRs between groups of lower-mass planets. These will become amenable to detection as observational techniques allow greater exploration of the lower-mass end of the extrasolar planet population.

6.5. Statistics of simulation outcomes

We now discuss the frequency with which certain simulation outcomes, such as planet-planet collisions, co-orbital system formation, *etc.* arose. Figure 10 displays the frequency with which co-orbital systems formed within the simulations, and survived for at least 10^5 years. The two leftmost bars show results for the 2D simulations presented in Paper I. The rightmost bars show results for the 3D runs presented in this paper. In the

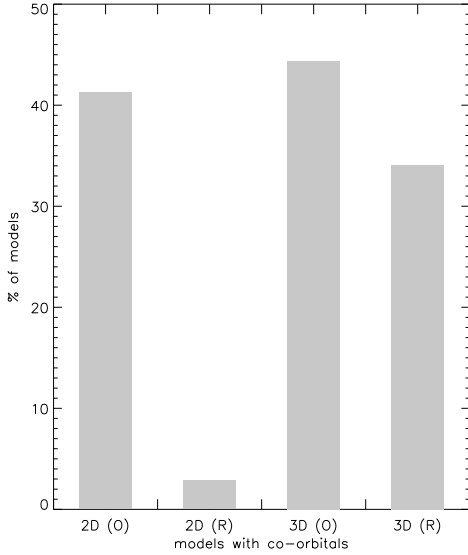


Fig. 10. Frequency of N -body models displaying stable horseshoe or tadpole planets. On the left, N -body data from Paper I is shown for comparison. Left–right: 2D ordered, 2D randomised, 3D ordered, 3D randomised.

cases where the protoplanet mass increased with increasing initial semi-major axis, we see that the 2D and 3D results are very similar, with $\sim 40\%$ of each set of calculations producing long-lived co-orbital systems. The situation for randomised mass distributions is different, however, with only 3% of 2D runs leading to co-orbital formation, whereas 34% of 3D runs resulted in long-term co-orbital formation. We believe this is due to a stronger eccentricity damping rate (in line with Tanaka & Ward 2004) in the 3D models, which allows the orbits of recently captured co-orbital bodies to be circularised and achieve a tadpole orbit sooner, reducing the probability of the body encountering a third protoplanet and being scattered from its horseshoe orbit. The effect is lessened among the models with initially ordered mass distributions because these favour large groups of protoplanets, meaning such a scattered body is likely to encounter further protoplanets and have multiple opportunities to be captured as a co-orbital entity.

Figure 11 shows the collision frequency for 2D and 3D simulations, as a function of the number of collisions occurring per simulation. The left hand charts show results for runs where the initial protoplanet mass increased with semi-major axis, the right hand charts show results for randomised mass distributions. Although there are small differences between both 2D and 3D runs, and between ordered and randomised mass distributions, the striking feature of these plots is their similarity. One normally expects that 2D and 3D simulations would produce different collision frequencies (with 2D runs leading to many more collisions), but this is not borne out by our results. The reason is most likely to be that the very strong inclination damping provided by the disc causes the planetary swarms to remain quasi-2D, thus increasing the collision frequency.

Figure 12 shows the frequency with which resonant groups form as a function of the number of protoplanets contained in the resonant group for 3D simulations only. Resonant groups are only counted in simulations if they survive for 10^5 years or more. The left hand chart is for models in which the initial planet mass

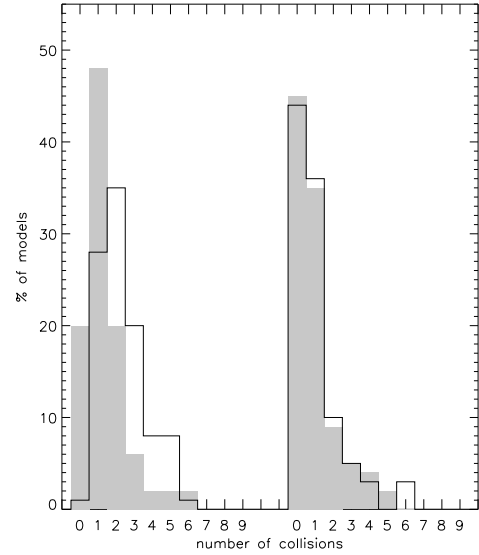


Fig. 11. Frequency of collisions per simulation for the ordered mass models (left) and randomised mass models (right). The open bars show the corresponding 2D data of Paper I.

increased with semi-major axis, and that on the right hand side is for the randomised mass distributions. The 3D runs show that simulations containing resonant groups of just two planets are most common, but with a significant number containing three to six planets. This is a clear indication that resonances involving smaller numbers of planets are more stable over the longer term.

7. Conclusions

We have performed simulations, using two different numerical schemes, which examine the evolution of swarms of low-mass protoplanets embedded in a 3D protoplanetary disc. First, we used hydrodynamical simulations to model the orbital evolution of planets on initially eccentric and/or inclined orbits, and fitted analytic equations for the rate of eccentricity and inclination damping, and migration, to these simulation results. These equations were then incorporated into an N -body code, which was used to perform many simulations of planetary swarms embedded in protoplanetary discs. We also performed a single hydrodynamic simulation of a planetary swarm embedded in a disc to verify the qualitative outcome of the N -body simulations. Although this simulation could not be evolved for as long as the N -body runs due to computational cost, we found basic agreement between it and the N -body simulations for the first $\approx 30,000$ years of evolution.

The main aim of this work was to re-examine previous results we had obtained using 2D simulations (see Paper I). It is known that type I migration of low-mass protoplanets may be slowed or even reversed by sustaining significant eccentricities (Papaloizou & Larwood 2000), and in Paper I we examined whether gravitational interactions between a swarm of protoplanets can provide the necessary excitation of eccentricity to prevent inward migration. The conclusion of that work was that disc-induced eccentricity damping is too strong, and ultimately protoplanetary swarms migrate into the central star. In this paper we have examined whether the inclusion of 3D effects changes this basic conclusion, as the dynamics in 3D can be quite differ-

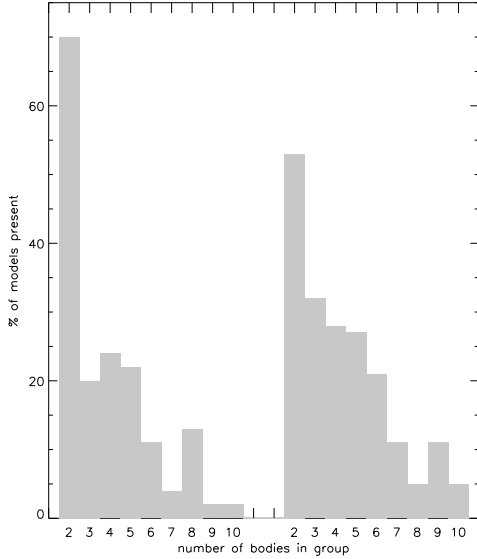


Fig. 12. Frequency of resonant group size per simulation for the ordered mass models (left) and randomised mass models (right).

ent. For example, the collision frequency may be reduced, and the possible excitation of significant inclination may assist in slowing down migration.

Our results indicate that the collision rate is reduced only marginally in 3D, because the strong disc-induced inclination damping causes the system to remain quasi-2D. We find that the disc-induced eccentricity damping remains too strong, so that a protoplanetary swarm is unable to maintain long epochs of strong gravitational scattering with concomitant high eccentricities.

Despite a wide variety of initial conditions, a typical mode of behaviour is observed across the models, which may be summarised as follows: Differential type I migration leads to converging orbits and a crowded system. Gravitational scattering leads to orbital exchanges between neighbouring planets, formation of groups of planets in mutual mean-motion resonances, formation of 1:1 co-orbital resonances, and occasional collisions. Smaller protoplanets are frequently scattered out beyond the population, but rarely achieve a semi-major axis greater than that of the initially outermost protoplanet prior to migration, nor an eccentricity or inclination capable of significantly prolonging their life times. Within $< 10^5$ yrs of commencement, the simulated system has typically settled down into a state with the protoplanets being in resonant groups, with each member of the group being in a mutual mean-motion resonance. These are usually first order mean-motion resonances, typically of degree 3:2–8:7. These resonant groups migrate inward in lockstep, to be accreted by the central star in the absence of a stopping mechanism such as an inner magnetospheric cavity. Occasionally a late burst of scattering activity occurs once a swarm of four or more bodies has migrated over several AU, but these systems always settle down to another phase of resonant migration that takes them to the star. A small, slowly migrating protoplanet may sometimes ($\approx 1\%$ of runs) be scattered to the outer edge of the swarm (where it cannot be trapped in resonance by a faster migrating body) and survive for $\sim 10^6$ yrs.

We conclude that if multiple protoplanets form coevally from oligarchic growth in the giant planet zone of a laminar disc, then

the long term evolution of the system will usually be collective inward migration and ultimate accretion by the central star. This occurs on a time scale much shorter than the accretion time required to accrete gaseous envelopes and end type I migration (Pollack et al. 1996; Papaloizou & Nelson 2005).

Co-orbital planets form as a natural consequence of gravitational scattering in crowded systems, and occur in more than one third of all models we have considered. Simulations performed with sub-Earth mass protoplanets showed that even very low-mass bodies could form and maintain co-orbital systems. We showed that an important factor in establishing these systems was the existence of a relatively flat disc surface density profile, which promotes convergence of planetary orbits through differential type I migration. We also showed that these co-orbital systems can be stable for over 3 billion years after gas disc dispersal. Co-orbital triples (i.e. three planets all in mutual 1:1 resonance) are also potentially viable, though none were found in the suite of simulations presented in this paper. Previous N -body simulations, using a slightly modified form for the eccentricity and damping formulae adopted in this paper, did result in such systems occasionally forming (Cresswell 2006). Although no planetary system is known to host such a configuration, we note that such ‘tadpole twins’ have been observed in orbit around Saturn, with Helene and Polydeuces occupying the L_4 and L_5 points of Dione (Murray et al. 2005). The observation of co-orbital extrasolar planet systems would be a strong indicator that a period of sustained dynamical relaxation had occurred during the formation of that system.

There are a number of open questions regarding the co-orbital planets that form in our simulations. The main issue is whether they can remain stable if one or both planets undergo gas accretion to become giants, since such a system would be more amenable to detection among the extrasolar planet population. Another question regarding our overall results is whether a combination of planet-planet interactions and stochastic migration, induced by turbulent density fluctuations in the disc (Nelson & Papaloizou 2004; Nelson 2005), can help prevent large-scale migration of some planets within the swarm. In particular, we find that mean-motion resonances are very effective in shielding the protoplanets from close-encounters that lead to scattering, and stochastic torques may increase the fragility of these resonances, including the co-orbitals. Another point of interest is the effect of other halting mechanisms for type I migration, such as a disc edge caused by a magnetospheric cavity (Terquem & Papaloizou 2007) or a ‘planet trap’ produced by a region of positive density gradient in the disc (Masset et al. 2006; Morbidelli et al. 2008), on a resonant group that has already formed and migrated some distance. Terquem & Papaloizou (2007) suggest that near-commensurabilities between protoplanets will survive beyond a disc edge, while experiments by Pierens & Nelson (2008) similarly indicate that a disc edge formed by the action of a close stellar binary companion can prevent the further migration of a moderate (~ 5) swarm of protoplanets, possibly subject to further reordering of the population. Our results suggest that the survival of co-orbital systems in such circumstances is possible, but depends on the rate at which migration is halted and any further scattering among the system. We will address these and other issues relating to planetary swarms and co-orbitals in a future paper.

Acknowledgements. The simulations reported here were performed using the UK Astrophysical Fluids Facility (UKAFF) and the QMUL HPC facility purchased under the SRIF initiative. We thank Doug McNeil for several interesting

discussions on the subject of co-orbital formation, and the anonymous referee for their constructive comments.

References

- Bodenheimer, P. & Pollack, J. B. 1986, *Icarus*, 67, 391
 Chambers, J. E. & Wetherill, G. W. 1998, *Icarus*, 136, 304
 Chambers, J. E., Wetherill, G. W., & Boss, A. P. 1996, *Icarus*, 119, 261
 Cresswell, P. 2006, PhD thesis, Queen Mary, University of London
 Cresswell, P., Dirksen, G., Kley, W., & Nelson, R. P. 2007, *A&A*
 Cresswell, P. & Nelson, R. P. 2006, *A&A*, 450, 833
 Gladman, B. 1993, *Icarus*, 106, 247
 Hayashi, C. 1981, *Progress of Theoretical Physics Supplement*, 70, 35
 Kley, W., Lee, M. H., Murray, N., & Peale, S. J. 2005, *A&A*, 437, 727
 Kley, W., Peitz, J., & Bryden, G. 2004, *A&A*, 414, 735
 Kokubo, E. & Ida, S. 2000, *Icarus*, 143, 15
 Lee, M. H. & Peale, S. J. 2002, *ApJ*, 567, 596
 Lovis, C., Mayor, M., Pepe, F., et al. 2006, *Nature*, 441, 305
 Masset, F. S., Morbidelli, A., Crida, A., & Ferreira, J. 2006, *ApJ*, 642, 478
 McNeil, D., Duncan, M., & Levison, H. F. 2005, *AJ*, 130, 2884
 Morbidelli, A., Crida, A., Masset, F., & Nelson, R. P. 2008, *A&A*, 478, 929
 Murray, C. D., Cooper, N. J., Evans, M. W., & Beurle, K. 2005, *Icarus*, 179, 222
 Nelson, R. P. 2005, *A&A*, 443, 1067
 Nelson, R. P. & Papaloizou, J. C. B. 2004, *MNRAS*, 350, 849
 Nelson, R. P., Papaloizou, J. C. B., Masset, F., & Kley, W. 2000, *MNRAS*, 318, 18
 Paardekooper, S.-J. & Mellema, G. 2006, *A&A*, 459, L17
 Papaloizou, J. C. B. & Larwood, J. D. 2000, *MNRAS*, 315, 823
 Papaloizou, J. C. B. & Nelson, R. P. 2005, *A&A*, 433, 247
 Papaloizou, J. C. B. & Szuszkiewicz, E. 2005, *MNRAS*, 363, 153
 Pierens, A. & Nelson, R. P. 2008, *A&A*, 478, 939
 Pollack, J. B., Hubickyj, O., Bodenheimer, P., et al. 1996, *Icarus*, 124, 62
 Press, W. H., Flannery, B. P., Teukolsky, S. A., & Vetterling, W. T. 1992, *Numerical Recipes in FORTRAN* (Cambridge University Press), p. 710
 Rivera, E. J., Lissauer, J. J., Butler, R. P., et al. 2005, *ApJ*, 634, 625
 Shakura, N. I. & Sunyaev, R. A. 1973, *A&A*, 24, 337
 Snellgrove, M. D., Papaloizou, J. C. B., & Nelson, R. P. 2001, *A&A*, 374, 1092
 Tanaka, H., Takeuchi, T., & Ward, W. R. 2002, *ApJ*, 565, 1257
 Tanaka, H. & Ward, W. R. 2004, *ApJ*, 602, 388
 Terquem, C. & Papaloizou, J. C. B. 2007, *ApJ*, 654, 1110
 Thommes, E. W. 2005, *ApJ*, 626, 1033
 Thommes, E. W., Duncan, M. J., & Levison, H. F. 2003, *Icarus*, 161, 431
 Udry, S., Bonfils, X., Delfosse, X., et al. 2007, *A&A*, 469, L43
 Ward, W. R. 1997, *Icarus*, 126, 261
 Zeigler, U. & Yorke, H. W. 1997, *Comput. Phys. Commun.*, 101, 54